Neuro-Oncology

Neuro-Oncology 18(11), 1579–1590, 2016
doi:10.1093/neuonc/now063
Advance Access date 21 April 2016

Restriction spectrum imaging predicts response to bevacizumab in patients with high-grade glioma

Carrie R. McDonald, Rachel L. Delfanti, Anitha P. Krishnan, Kelly M. Leyden, Jona A. Hattangadi-Gluth, Tyler M. Seibert, Roshan Karunamuni, Pia Elbe, Joshua M. Kuperman, Hauke Bartsch, David E. Piccioni, Nathan S. White, Anders M. Dale, and Nikdokht Farid

Department of Psychiatry, University of California, San Diego, La Jolla, California (C.R.M., A.M.D.), Department of Radiology, University of California, San Diego, La Jolla, California (R.L.D., J.M.K., H.B., N.S.W., A.M.D., N.F.), Department of Radiation Medicine, University of California, San Diego, La Jolla, California (C.R.M., J.A.H.-G., T.M.S., R.K.), Department of Neurosciences, University of California, San Diego, La Jolla, California (D.E.P., A.M.D.), Multimodal Imaging Laboratory, University of California, San Diego, La Jolla, California (C.R.M., A.P.K., K.M.L., T.M.S., P.E., J.M.K., H.B., N.S.W., A.M.D., N.F.)

Corresponding Author: C. R. McDonald, PhD, Multimodal Imaging Laboratory, Suite C101; 8950 Villa La Jolla Drive, La Jolla, CA 92037 (camcdonald@ucsd.edu).

Background. Diffusion-weighted imaging has shown initial promise for evaluating response to bevacizumab in patients with high-grade glioma (HGG). However, it is well recognized that the apparent diffusion coefficient (ADC) is influenced by bevacizumab-induced reductions in edema, which may limit its prognostic value. We demonstrate that an advanced diffusion-weighted imaging technique, restriction spectrum imaging (RSI), improves the evaluation of response to bevacizumab because unlike ADC, RSI is not affected by resolution of edema.

Methods. RSI and ADC maps were analyzed for 40 patients with HGG prior to and following initiation of bevacizumab. Volumes of interest were drawn for regions of contrast enhancement (CE) and fluid attenuated inversion recovery (FLAIR) hyperintensity and histogram percentiles within volumes of interest were calculated for ADC 10th percentile (ADC-$CE_{10\%}$, ADC-$FLAIR_{10\%}$) and for RSI 90th percentile (RSI-$CE_{90\%}$, RSI-$FLAIR_{90\%}$). Cox proportional hazard models were used to evaluate the relationship between imaging parameters, progression-free survival (PFS), and overall survival (OS).

Results. An increase in RSI-$FLAIR_{90\%}$ following bevacizumab was the strongest predictor of poor PFS ($P = .016$) and OS ($P = .004$), whereas decreases in ADC-$FLAIR_{10\%}$ showed a weaker association with OS only ($P = .041$). Within the CE region, increases in RSI-$CE_{90\%}$ alone were associated with poorer OS. Correlational analysis revealed that decreases in FLAIR volume were associated with decreases in ADC-$FLAIR_{10\%}$, but not with changes in RSI-$FLAIR_{90\%}$.

Conclusion. RSI is less influenced by changes in edema, conferring an advantage of RSI over ADC for evaluating response to anti-angiogenic therapy in patients with HGG.

Keywords: apparent diffusion coefficient, bevacizumab, diffusion-weighted imaging, high-grade glioma, restriction spectrum imaging.

High-grade gliomas (HGGs) are hypervascular tumors that account for nearly 80% of malignant primary brain tumors in adults and portend a very poor prognosis. Glioblastoma (GBM) is the most common and aggressive HGG, with the most dismal survival: only 12–14 months.[1] Standard treatment for newly diagnosed HGGs is a combination of surgical resection followed by concurrent radiotherapy and chemotherapy with temozolomide.[2] However, despite best available treatment, recurrence rates are nearly 100%. Anti-angiogenic agents are commonly used in recurrent HGG due to early data that demonstrated improved progression-free survival (PFS) and objective response rate in patients treated with bevacizumab.[3–5] This monoclonal vascular endothelial growth factor (VEGF)–blocking antibody functions to normalize vascular permeability and regulate angiogenesis in patients with HGG. As a result, post-bevacizumab-treated tumors may exhibit a sharp decrease in contrast enhancement (CE) and fluid-attenuated inversion recovery (FLAIR) hyperintensity without a comparable tumor

Received 25 January 2016; accepted 18 March 2016

response—a phenomenon known as pseudoresponse.[6] This response reduces the utility of conventional imaging measures because reductions in CE and FLAIR hyperintensity may be due to either an antipermeability effect or to a reduction in tumor volume.[7] With recent phase III studies suggesting no overall survival (OS) benefit for patients treated with bevacizumab plus lomustine over lomustine alone,[8] it is becoming increasingly important to identify early imaging biomarkers that can differentiate responders from nonresponders.

Diffusion-weighted imaging (DWI) has been proposed as a noninvasive imaging marker for evaluating tumor response in the setting of treatment with anti-angiogenic therapy.[9–12] Specifically, the apparent diffusion coefficient (ADC), a quantitative DWI metric that characterizes the random motion of water molecules within a voxel, has been shown to inversely correlate with tumor cell density in patients with HGG.[13] Decreases in ADC are thought to reflect increased cellularity (ie, aggressive tumor), whereas increases in ADC have been proposed to reflect reduced cellularity (ie, a treatment response). However, it is increasingly recognized that edema and tumor-related necrosis also increase ADC values.[14] Because ADC represents a composite of *hindered* diffusion within the extracellular matrix and *restricted* diffusion within tumor cells, decreases in ADC are highly related to the reabsorption of edema after treatment. It follows that the influence of edema on ADC values can complicate the interpretation of treatment response following bevacizumab, and subsequently ADC remains a nonspecific measure of tumor cellularity.[7]

To account for the potential influence of edema and other nontumor tissue on the ADC signal, a number of statistical methods have been proposed. Pope et al[10,15] and Ellingson et al[16] applied a double Gaussian mixed model to ADC values within the CE tumor, under the assumption that the upper histogram likely reflects a mixture of tumor, necrotic tissue, and edema, whereas the lower histogram likely reflects solid tumor. Other investigators have applied a 4-component curve-fitting model of ADC histograms within CE and FLAIR/T2 regions to remove the influence of nontumor tissue.[17] More recently, traditional and graded functional diffusion maps (fDMs) have been employed that characterize different thresholds of ADC change on a voxelwise basis in order to estimate cellularity changes occurring in subportions of the tumor.[18–21] Collectively, these methods demonstrate initial promise in the prediction and evaluation of response to bevacizumab; however, results have occasionally been conflicting, with some studies reporting that a *lower* ADC is associated with shorter PFS and OS[10,15,16,22] and others reporting that a *higher* ADC is associated with shorter PFS and OS.[20,23] Although the reason for opposing findings is not entirely clear, a more direct marker of tumor cellularity within the voxel itself (eg, restricted diffusion *within* cells) that is not influenced by edema and other pathologies in the extracellular matrix would greatly simplify the interpretation of DWI changes and could improve the evaluation of treatment response.

We have introduced an advanced DWI technique called *restriction spectrum imaging* (RSI) that maximizes sensitivity to the restricted diffusion signal within tumor cells while excluding the hindered diffusion signal associated with edema.[24] Whereas ADC reflects both hindered and restricted diffusion pools within a voxel, RSI uses multiple b-values and diffusion directions (ie, "multi-shell" diffusion data) to separate out the spherically restricted water compartment within tumor cells from the restricted and hindered water within neurites and the extracellular space, respectively. Previously, we demonstrated that RSI provides improved tumor conspicuity relative to ADC and high b-value DWI (b = 4000) in patients with primary and metastatic brain tumors[25] and it was shown to be more robust to changes in edema following treatment with bevacizumab.[26] However, whether RSI can provide a more accurate biomarker of response to anti-angiogenic therapy compared with standard ADC and conventional imaging has not been evaluated.

In this study, we evaluate the ability of RSI to quantify response to therapy in 40 patients with HGG treated with bevacizumab relative to ADC, postcontrast, and FLAIR measures. Based on recent data demonstrating that the ADC 10th percentile within the FLAIR/T2 lesion is the strongest predictor of PFS and OS compared with other common metrics (ie, change in ADC from traditional and graded fDMs; ADC obtained from 2-mixture normal fitting in the CE lesion) following bevacizumab,[7] we chose to use this ADC metric and comparable RSI values in our analysis. We evaluate diffusion changes within both the CE and the FLAIR/T2 regions due to evidence that bevacizumab may effectively control CE tumor while leading to a more infiltrative pattern of tumor growth in nonenhancing regions.[12,27–29] In line with our previous work,[25,26,30,31] we hypothesized that changes in RSI would be minimally affected by bevacizumab-induced reductions in edema, whereas changes in ADC would be highly influenced by treatment-related reductions in edema due to ADC sensitivity to fast, hindered diffusion. We hypothesized that RSI's ability to distinguish cellularity from edema would make it a stronger predictor of PFS and OS relative to existing measures.

Methods

Patients

All patients included in this retrospective study signed consent forms approved by the institutional review board. From April 2011 to March 2015, 60 patients with HGG were identified who had both pre- and post-bevacizumab MRIs that included our standardized RSI sequence. From this group, 40 patients met the following inclusion criteria to form the final study cohort (see Table 1 and Supplementary Figure): (i) HGG treated with bevacizumab for tumor recurrence, (ii) at least one baseline RSI scan prior to initiating bevacizumab therapy (median = 32 days; range = 1–55 days) and a follow-up RSI scan within the first 1–2 months of treatment (median = 14 days; range = 1–58 days), and (iii) no significant blood products on susceptibility-weighted images. Patients were excluded for the following reasons: they received bevacizumab for reasons other than recurrent tumor (eg, radiation necrosis; $N = 9$), the baseline RSI scan was >2 months prior to initiating bevacizumab therapy ($N = 2$), significant artifacts on imaging were present that would have affected the diffusion signal ($N = 5$), or the complete RSI or conventional imaging sequence was not available at one of the 2 timepoints ($N = 4$). To our knowledge, all patients tolerated the scan session well. None of the patients showed significant artifacts due to excessive motion. Thirty-four patients had pathologically confirmed GBM,

Table 1. Demographic and clinical characteristics of the patient sample

Patient ID	Age	Sex	Pathology	Therapy Type	Total Pre-Bevacizumab Surgeries	Pre-Bevacizumab Surgical Extent	IDH1 Status	EGFR Amplification	Steroid Dose Pre-Bevacizumab (mg/d)[a]	Steroid Dose Post-Bevacizumab (mg/d)[a]	PFS (mo)	OS (mo)	Malignant Transformation
1	49	M	GBM[b]	BEV + CARBO	3[c]	GTR			6	12	3.94	3.06	
2	63	F	GBM[b]	BEV + TMZ	2	STR			0	0	7.75	5.03	
3	58	F	GBM	BEV + IRINOTECAN	1	STR		N	1	1	1.38	7.69	
4	59	F	GBM	MONO	1	GTR	WT		4	4	4.17	11.63	
5	56	M	GBM	BEV + CARBO	1	STR			2	2	3.58	9.86	
6	73	M	GBM	MONO	1	GTR			2	2	3.02	21.82	
7	53	F	GBM	BEV + CCNU	2	GTR			1	1	7.43	6.9	
8	77	F	GBM	BEV + TMZ	1	STR	WT	Y	4	4	15.24	11.79	
9	65	M	GBM	BEV + CCNU	3	STR	WT	Y	2	2	6.44	6.9	
10	61	M	GBM	BEV + CCNU	2[c]	STR	WT		0	4	11.73	1.54	
11	36	M	AO[b]	MONO	2	STR	WT	N	2	2	5.16	8.08	Y
12	54	M	GBM	BEV + DASATINIB	1	GTR		N	1	8	1.54	10.81	
13	65	M	GBM	MONO	2	GTR	WT	N	6	6	7.1	4.6	
14	44	M	AO	BEV + TMZ	1	GTR			2	4	7.92	7.52	
15	49	F	GBM	BEV + DASATINIB	1	STR	WT	N	16	2	2.66	13.57	
16	34	M	GBM[b]	BEV + CARBO	2	STR			2	6	3.61	2.96	
17	60	F	GBM	MONO	1	STR		N	4	4	11.47	6.8	
18	53	M	GBM	MONO	2	STR	WT	Y	2	2	0.92	4.86	
19	63	M	GBM	MONO	1	GTR	WT	Y	8	2	6.24	19.32	
20	62	M	AO	BEV + IRINOTECAN	5	STR	MUT	N	4	8	3.45	8.61	Y
21	49	M	AA	MONO	2	STR	WT	Y	0	0	19.32	10.84	Y
22	46	M	GBM	BEV + SINGLE CCNU	4	GTR	WT	Y	4	2	5.13	4.27	
23	81	F	GBM	MONO	1	GTR			2	2/1 QOD	2.17	18.17	
24	45	M	GBM[b]	BEV + CCNU	2	STR	MUT	N	1	2	2.53	17.58	
25	55	M	GBM	MONO	1	STR			12	4	15.47	7.36	
26	33	F	AA	MONO	1	STR	MUT	N	0	4	1.84	2.27	
27	58	M	AA	MONO	1	STR			8	16	1.84	2.37	
28	61	M	GBM	BEV + CCNU	1	GTR	WT		6	6	1.58	6.67	
29	31	F	GBM[b]	MONO	2	GTR		N	2/1 QOD	2/1 QOD	2.37	4.4	
30	65	M	GBM	MONO	2	STR	WT	Y	8	8	6.67	4.24	
31	74	M	GBM	MONO	1	GTR	WT	Y	6	6	4.3	6.21	
32	66	M	GBM	BEV + TMZ	1	STR			6	1.75	2.69	9.92	
33	53	M	GBM	MONO	1	STR			0	8	5.85	4.37	
34	37	M	GBM	BEV + TMZ	2	STR			0	0	2.99	3.38	

Continued

Table 1. *Continued*

Patient ID	Age	Sex	Pathology	Therapy Type	Total Pre-Bevacizumab Surgeries	Pre-Bevacizumab Surgical Extent	IDH1 Status	EGFR Amplification	Steroid Dose Pre-Bevacizumab (mg/d)[a]	Steroid Dose Post-Bevacizumab (mg/d)[a]	PFS (mo)	OS (mo)	Malignant Transformation
35	65	M	GBM	BEV + CARBO	2	GTR			2	8	0.23	23.56	
36	59	M	GBM[b]	BEV + CARBO	2	STR		Y	1	1.5	0.99	7.72	
37	61	F	GBM	BEV + CARBO	2[c]	STR	WT	Y	0[d]	16	12.85	5.09	
38	58	F	GBM	MONO	2	GTR		N	0	0	5.29	1.18	
39	67	M	GBM	MONO	1	GTR			2	1.5	2.1	155	
40	69	F	GBM	BEV + TMZ	2	STR			0	8	1.18	36	

Abbreviations: AO, anaplastic oligodendroglioma; AA, anaplastic astrocytoma; BEV, bevacizumab; CARBO, carboplatin; TMZ, temozolomide; MONO, monotherapy; CCNU.
[a]Decadron dosage during time of MRI scan.
[b]Pathology diagnosis at time of recurrence; WT, wild type; MUT, mutant.
[c]Patient received an additional surgery after bevacizumab treatment; GTR, gross total resection; STR, subtotal resection.
[d]Prednisone 60 mg/day for 5 days, no Decadron.

whereas 3 had anaplastic astrocytomas and 3 had anaplastic oligodendrogliomas. In 20 patients, epidermal growth factor receptor (EGFR) amplification status was available (10 patients were EGFR amplified [EGFR+] and 10 patients were EGFR non-amplified [EGFR−]). The average age of the final cohort was 57.3 years, ranging from 31 to 81 years, with 27 males and 13 females. All patients were initially treated with surgery followed by chemoradiation with temozolomide (alone or in combination with other agents). Upon first or second recurrence, 18 patients received bevacizumab monotherapy, whereas 22 received bevacizumab in combination with other agents (carboplatin, irinotecan, CCNU, temozolomide). All patients underwent at least one surgery (maximum of 5) prior to treatment with bevacizumab, with the most recent surgery before the initiation of bevacizumab being a subtotal resection (STR) in 24 patients and a gross total resection (GTR) in 16 patients. Surgery type at this timepoint was used to determine the extent of resection in the analysis. To further avoid contamination from immediate postsurgical effects such as hemorrhage, no MRIs obtained within the first 2 months following surgery were included in the study.

Definition of PFS/OS

For all patients included in the study, PFS and OS were calculated from the initiation of bevacizumab to tumor progression or death, respectively. Tumor progression was confirmed by direct pathologic confirmation when available ($N = 7$), or unequivocal evidence of progression based on MRI and neurological status ($N = 33$) by a board-certified neuroradiologist who was blinded to steroid use (N.F.) using the Response Assessment in Neuro-Oncology (RANO) criteria.[32]

MR Imaging

MRI was performed on a 3.0 T GE Signa Excite HDx scanner equipped with an 8-channel head coil. The imaging protocol included pre- and postgadolinium 3D volumetric T1-weighted inversion recovery–spoiled gradient recalled echo (IR-SPGR) sequences (echo time [TE]/repetition time [TR] = 2.8/6.5 ms; inversion time [TI] = 450 ms; flip angle [FA] = 8 degrees; field of view [FOV] = 24 cm; 0.93 × 0.93 × 1.2 mm) and a 3D T2-weighted FLAIR sequence (TE/TR = 126/6000 ms; TI = 1863 ms; FOV = 24 cm; 0.93 × .093 × 1.2 mm). For RSI, a single-shot pulsed-field gradient spin-echo echo-planar imaging sequence was used (TE/TR = 96 ms/17 s; FOV = 24 cm, matrix = 128 × 128 × 48; slice thickness = 2.5 mm) with 4 b-values (b = 0, 500, 1500, and 4000 s/mm^2), and 6, 6, and 15 unique diffusion directions for each nonzero b-value, respectively (28 total volumes, ~8 min scan time).

Preprocessing, ADC, and RSI Calculation

Prior to analysis, raw data were corrected for geometric distortions due to susceptibility, gradient nonlinearities, and eddy currents using in-house software.[33] This was followed by correction of patient motion using in-house software. ADC values were calculated from a tensor fit to the full dataset (b = 0, 500, 1500, and 4000 s/mm^2). Three b-values were utilized per the recommendations of the National Cancer Institute Diffusion

MRI Consensus Conference for estimation of perfusion-insensitive ADC.[34]

RSI utilizes a multiple b-shell acquisition in conjunction with a linear mixture model to isolate diffusion signals from separable hindered and restricted diffusion compartments within a voxel. Technical details describing the RSI mathematical framework are described in full elsewhere.[24,25,35] In this study, the measured signal in each voxel was written as the sum of signals from 4 distinct tissue compartments: (i) the signal from water trapped within small spherical cells that is restricted in all directions, (ii) the signal from water trapped in elongated neural processes (ie, neurites) that is restricted in the transverse direction, (iii) the signal from extracellular water that is hindered by cells and neural processes, and (iv) the signal from free water residing in CSF-filled compartments. The orientation distributions of anisotropic compartments (ii, iii) were modeled using 4th order spherical harmonics. Estimates of the signal fractions of each compartment and respective spherical harmonics parameters were obtained using least-squares estimation with Tikhonov regularization.[24,25] RSI "cellularity" estimates were computed by combining the signal fraction from the intracellular compartment (i) with the isotropic restricted component of the neurite compartment (ii). The latter component was included to maximize sensitivity to isotropic restricted diffusion within peritumoral white matter. The RSI cellularity maps were finally transformed to a standard *Z*-score by scaling each patient's data by the population mean and standard deviation in normal-appearing white matter derived from the entire patient sample.

Longitudinal Registration

The pre- and postcontrast 3D IR-SPGR images and FLAIR images were rigidly registered to each other at the 2 timepoints and affine registered between timepoints. The precontrast IR-SPGR images, weighted by T2-weighted FLAIR to correct for regions of hypointensity, were used to guide the registration, and the computed deformations were then applied to the coregistered RSI and ADC volumes.

Volumes of Interest and Histogram Analysis

CE volumes (CE_{vol}) and FLAIR hyperintensity volumes ($FLAIR_{vol}$) excluding the necrotic core and resection cavity were segmented semi-automatically (Amira software package, Visage Imaging) on the coregistered postcontrast 3D IR-SPGR images and FLAIR images acquired both pre- and posttreatment. The final $FLAIR_{vol}$ also excluded the CE_{vol} in order to obtain an estimate of the nonenhancing lesion. All volumes of interest (VOIs) were drawn by 2 trained image analysts (R.D. and K.L.) and approved by a board-certified neuroradiologist with expertise in neuro-oncology. Histograms of ADC and RSI cellularity values were generated within the pre- and post-bevacizumab VOIs. Based on previous work,[7] the ADC 10th percentile was selected for each patient for inclusion in the analysis. Because ADC and RSI values are inversely related (ie, *lower* ADC values and *higher* RSI cellularity values are related to high tumor cellularity), this corresponded to the 90th percentile value of the RSI cellularity histogram. Imaging metrics included in the analysis were the pre-bevacizumab, post-bevacizumab, and pre-post *change* values for each of the following: $FLAIR_{vol}$, CE_{vol}, the 90th percentile of RSI cellularity values in the CE ($RSI\text{-}CE_{90\%}$) and FLAIR ($RSI\text{-}FLAIR_{90\%}$) VOIs, and the 10th percentile of ADC in the CE ($ADC\text{-}CE_{10\%}$) and FLAIR ($ADC\text{-}FLAIR_{10\%}$) VOIs.

Statistical Analysis

Univariate Cox proportional hazard (CPH) models were used to determine the contribution of clinical variables (age, gender, extent of resection [STR, GTR], tumor grade, steroid dose, and treatment regimen [bevacizumab monotherapy vs bevacizumab combination therapy]) to PFS and OS. Multivariate CPH models (with 1000 bootstrap samples) that included significant clinical covariates were employed to determine the relationship between (i) pre-bevacizumab, (ii) post-bevacizumab, and (iii) pre-post change in each imaging metric and PFS/OS. Classification and regression tree (CART) analysis was used to determine the optimal cutoff for dichotomizing the RSI and ADC metrics obtained from the CPH models. Kaplan–Meier survival analyses were then conducted based on the subgroups obtained from the CART split and compared using a log-rank test. In a subanalysis, EGFR status was added to the CPH model that included the imaging metrics to determine whether this molecular information enhanced the prediction of PFS and OS. Furthermore, there are some preliminary data to suggest that high b-value DWI may improve the evaluation of pseudoresponse in patients treated with bevacizumab relative to standard b-value ADC/DWI due to the decreased sensitivity to fast diffusion (ie, edema) at higher b-values.[36] Therefore, in a second subanalysis, RSI was further compared with high b-value DWI ($b = 4000$). In the case of no progression or death, the event time was censored at the date of last contact. In all cases, 2-tailed $P < .05$ was considered statistically significant (SPSS package).

Results

Clinical

Median PFS and OS for the patient cohort from the start of bevacizumab was 3.8 months and 6.9 months, respectively. Based on RANO criteria, 38 patients (95%) showed tumor progression by study completion and 30 patients (75%) were deceased at last follow-up. Of all of the clinical variables, only greater extent of resection (ie, GTR) was significantly associated with improved PFS (hazard ratio [HR] = 1.5, 95% CI = .78–3.1; $P < .05$) and OS (HR = 1.6, 95% CI = .76–3.4; $P < .05$), and therefore it was included in all multivariate CPH analyses.

CE and FLAIR Volumes

At the group level, there was a significant decrease in both CE_{vol}, $t(39) = 7.1$, $P < .001$, and $FLAIR_{vol}$, $t(39) = 3.8$, $P < .01$, following the initiation of bevacizumab therapy. Multivariate CPH models revealed that none of the $FLAIR_{vol}$ or CE_{vol} values were significantly associated with PFS or OS (see Table 2).

Figure 1 shows examples of 2 patients at baseline and on treatment with bevacizumab. Figure 1A demonstrates an example of poor response to therapy (short PFS and OS), whereas Fig. 1B shows a good response (long PFS and OS). Across a majority of the patients, areas of restricted diffusion appeared

Table 2. Summary of multivariate CPH models with surgical extent (subtotal, gross total resection) as a covariate

Parameter	Timepoint	PFS		OS	
		P-value	HR (95% CI)	*P*-value	HR (95% CI)
CE_{vol}	Pre-bevacizumab	.841	1.00 (1.00 1.02)	.094	1.00 (1.00 1.02)
	Post-bevacizumab	.501	1.00 (1.00 1.00)	.198	1.00 (1.00 1.00)
	Pre-post Δ	.658	1.02 (0.99 1.00)	.538	1.03 (0.99 1.05)
$FLAIR_{vol}$	Pre-bevacizumab	.470	1.00 (1.00 1.00)	.412	1.00 (0.98 1.01)
	Post-bevacizumab	.916	1.04 (0.95 1.02)	.297	1.00 (1.00 1.00)
	Pre-post Δ	.086	1.00 (0.90 1.00)	.851	1.00 (1.00 1.00)
RSI-$CE_{90\%}$	Pre-bevacizumab	.114	1.27 (0.91 1.78)	.285	1.18 (0.82 3.93)
	Post-bevacizumab	.138	1.27 (0.96 1.67)	***.016****	1.38 (1.03 1.86)
	Pre-post Δ	.435	1.31 (0.85 1.49)	.073	1.37 (0.97 1.94)
RSI-$FLAIR_{90\%}$	Pre-bevacizumab	.180	1.21 (0.89 1.64)	.127	1.23 (0.88 1.71)
	Post-bevacizumab	***.013****	1.54 (1.02 2.21)	***.007*****	1.57 (1.09 2.26)
	Pre-post Δ	***.016****	1.65 (0.98 2.77)	***.004*****	2.00 (1.19 3.37)
ADC-$CE_{10\%}$	Pre-bevacizumab	.369	0.99 (0.99 1.00)	.776	0.99 (0.99 1.00)
	Post-bevacizumab	.795	0.99 (0.99 1.01)	.978	1.00 (0.99 1.01)
	Pre-post Δ	.318	1.00 (0.99 1.01)	.746	1.00 (0.99 1.01)
ADC-$FLAIR_{10\%}$	Pre-bevacizumab	.711	1.00 (0.99 1.01)	.990	1.00 (0.99 1.01)
	Post-bevacizumab	.186	0.99 (0.98 1.00)	***.035****	0.99 (0.98 1.00)
	Pre-post Δ	.147	1.00 (0.99 1.01)	***.041****	0.99 (0.98 0.99)

*$P < .05$ and **$P < .01$.

more conspicuous on the RSI cellularity maps (RSI-CMs) relative to ADC both at baseline and following treatment. ADC signal intensity following treatment (ie, when the surrounding FLAIR hyperintensity has partially resolved) became difficult to distinguish from normal-appearing white matter in many patients. Furthermore, the large region of decreased signal intensity on ADC following treatment often mirrored the area of decreased signal intensity on the FLAIR image, whereas RSI intensity changes did not appear to reflect the area of decreased FLAIR hyperintensity.

RSI and ADC Metrics

Paired *t*-tests demonstrated a significant decrease in the ADC-$FLAIR_{10\%}$, $t(39) = 9.3$, $P < .001$, and ADC-$CE_{10\%}$, $t(39) = 8.9$, $P < .001$, following treatment with bevacizumab, whereas there was an increase in RSI-$FLAIR_{90\%}$ post-bevacizumab, $t(39) = -2.3$, $P < .05$, with no significant change in RSI-$CE_{90\%}$, $t(39) = 1.4$, $P = .169$, at the group level. At the individual subject level, 70% of patients showed a decrease of >10% in the ADC-$CE_{10\%}$ and 66% showed a decrease of >10% in the ADC-$FLAIR_{10\%}$. No patients showed an increase in ADC in either region. Conversely, 28% of patients showed a >10% increase and 40% showed a >10% decrease in the RSI-$CE_{90\%}$. In the RSI-$FLAIR_{90\%}$, 47% showed an increase and 7% showed a decrease that exceeded 10%.

Multivariate CPH models indicated that none of the pre-bevacizumab RSI or ADC values predicted PFS or OS (see Table 2). Rather, within the FLAIR/T2 region, the RSI-$FLAIR_{90\%}$ post-bevacizumab and the change in RSI-$FLAIR_{90\%}$ were associated with both PFS and OS. In addition, the post-bevacizumab and the change in ADC-$FLAIR_{10\%}$ were associated with OS, but not with PFS. Greater increase in RSI values and greater decrease in ADC values within the FLAIR hyperintense region were associated with poorer survival. In the CE region, only the post-bevacizumab RSI-$CE_{90\%}$ was significant, such that higher RSI values were associated with poorer OS. Given that both the change in ADC-$FLAIR_{10\%}$ and RSI-$FLAIR_{90\%}$ were associated with survival, a stepwise CPH model was performed with both variables to determine whether these variables contributed unique variance versus whether one variable was a stronger predictor of survival. This analysis demonstrated that only RSI-$FLAIR_{90\%}$ was retained in the model for both PFS (HR = 1.74, CI = 1.0–2.9; $P < .05$) and OS (HR = 1.80, CI = 1.3–3.5; $P < .05$). Furthermore, Pearson correlations revealed that the decrease in ADC-$FLAIR_{10\%}$ was associated with a decrease in $FLAIR_{vol}$ ($r = .41$, $P < .05$), whereas there was no association between change in RSI-$FLAIR_{90\%}$ and $FLAIR_{vol}$ ($r = -0.08$, $P > .05$; Fig. 2). In addition, there was no association between steroid doses at baseline or follow-up and changes in any of the ADC or RSI values (all *P*-values >.05).

CART analysis was performed to identify optimal cut-points for change in RSI-$FLAIR_{90\%}$ and change in ADC-$FLAIR_{10\%}$ that could provide clinically relevant information regarding early response to therapy. An RSI-$FLAIR_{90\%}$ change value of 0.120 was determined to best dichotomize patients into 2 groups for PFS, whereas an ADC-$FLAIR_{10\%}$ change value of −50.0 was determined to best dichotomize patients for PFS. Kaplan–Meier survival curves revealed that the CART-determined RSI cutoff significantly stratified the groups for both PFS [log-rank χ^2 (1) = 7.3, $P = .007$] and OS [log-rank χ^2 (1) = 7.6, $P = .004$], categorizing 11 patients with a more favorable outcome and 29 patients with a less favorable outcome. Conversely, the CART-determined ADC cutoff did not significantly stratify patients

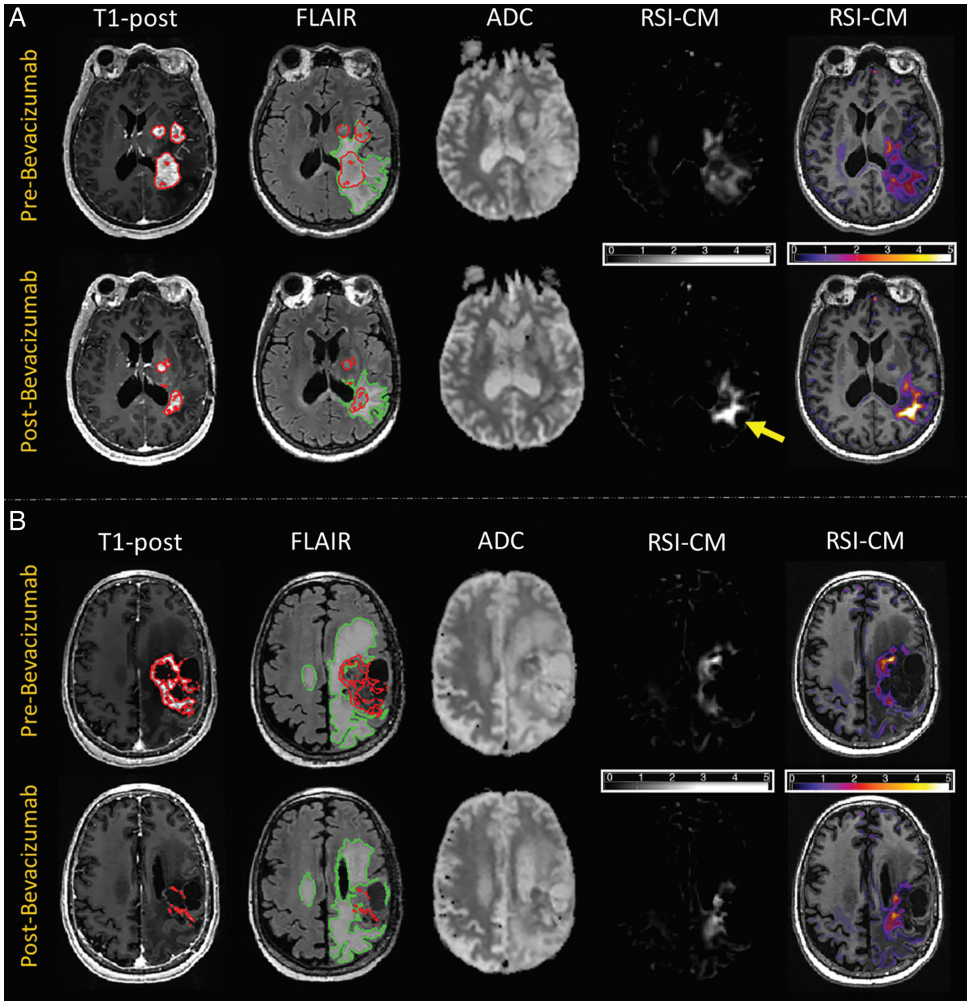

Fig. 1. T1-postcontrast, FLAIR, ADC, and RSI cellularity *Z*-score maps (RSI-CMs) for 2 patients pre- and post-bevacizumab. Images at far right show the RSI-CMs as a color overlay on a T1-weighted image to provide better anatomic detail. (A) A 58-year-old female status post STR followed by chemoradiation for a left parietal GBM. VOIs for CE and FLAIR are delineated with the red and green contours, respectively. Comparison of MRI 13 days before initiation of bevacizumab and 42 days post-bevacizumab demonstrates decrease in volume of CE and FLAIR hyperintensity. However, on the post-bevacizumab image, within the region of FLAIR hyperintensity, the region of low ADC is difficult to distinguish from the surrounding normal-appearing white matter, whereas the signal on the RSI-CM is more conspicuous and is increased from the pre-bevacizumab scan (yellow arrow), suggestive of a poor outcome. Patient had poor PFS and OS, with PFS of 43 days and OS of 93 days. (B) A 55-year-old male status post STR followed by chemoradiation for a left frontoparietal GBM. VOIs for CE and FLAIR are delineated with the red and green contours, respectively. Comparison of MRI 14 days before initiation of bevacizumab and 26 days post-bevacizumab demonstrates significant decrease in CE with a more modest decrease in FLAIR hyperintensity. However, on the post-bevacizumab image, within the region of FLAIR hyperintensity, there is minimal decrease in both ADC as well as on the RSI-CM. While the decrease in ADC is discordant, the decrease in RSI is suggestive of a better outcome, which is validated by the patient's good survival (still alive with OS >553 days).

for PFS [log-rank χ^2 (1) = 1.9, $P = .168$], and only marginally stratified patients for OS [log-rank χ^2 (1) = 5.7, $P = .04$] (Fig. 3), categorizing 15 patients with a favorable outcome and 25 patients with unfavorable outcome.

EGFR Amplification Status

A post-hoc CPH analysis revealed that EGFR amplification status was associated with both PFS (HR = 3.10, $P < .05$) and OS (HR = 3.14, $P < .05$). Kaplan–Meier curves show that EGFR+ patients had longer PFS [log-rank χ^2 (1) = 4.76, $P < .05$] and OS [log-rank χ^2 (1) = 474, $P < .05$] relative to EGFR– patients following treatment with bevacizumab (Fig. 4). However, EGFR status did not add to a multivariate CPH model with RSI-FLAIR$_{90\%}$ included (model change $P > .05$). Rather, chi-square tests stratifying EGFR+ and EGFR– patients into those with high versus low changes in RSI-FLAIR$_{90\%}$ (based on the CART split) revealed a significant difference in the proportion of patients in each cell [χ^2 (1) = 4.1, $P < .05$]. All EGFR– patients showed increased RSI-FLAIR$_{90\%}$ and poor PFS/OS post-bevacizumab, whereas the EGFR+ patients were a more heterogeneous group (6 were in the high RSI-FLAIR$_{90\%}$ change

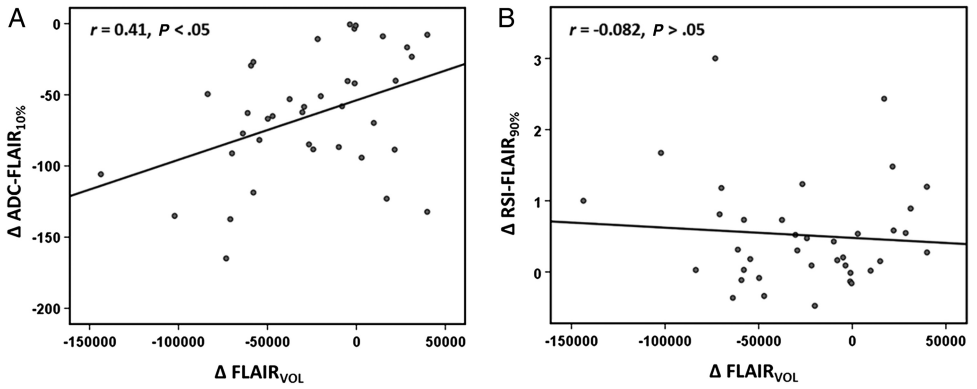

Fig. 2. Scatterplots of the relationship between change in $FLAIR_{vol}$ and changes in (A) ADC-$FLAIR_{10\%}$ and (B) RSI-$FLAIR_{90\%}$. $FLAIR_{vol}$ is measured in mm^3, ADC is measured in $\mu m^2/s$, and RSI is measured in cellularity units.

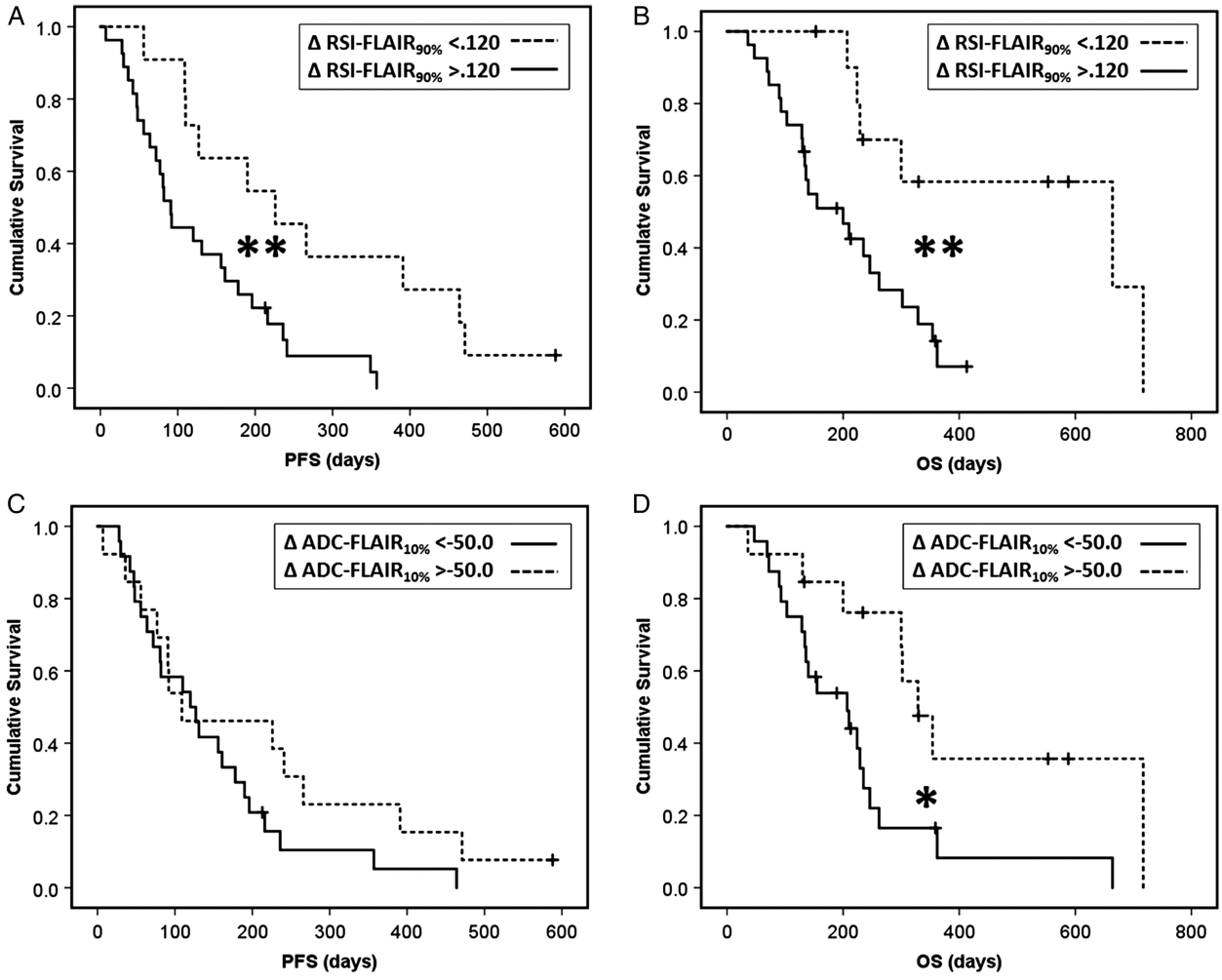

Fig. 3. Stratification of patients based on the CART analysis for splits in RSI-$FLAIR_{90\%}$ and ADC-$FLAIR_{10\%}$. Kaplan–Meier curves for high and low change groups for RSI-$FLAIR_{90\%}$ (A, B) and for high and low change groups for ADC-$FLAIR_{10\%}$ (C, D). $^*P < .05$, $^{**}P < .01$.

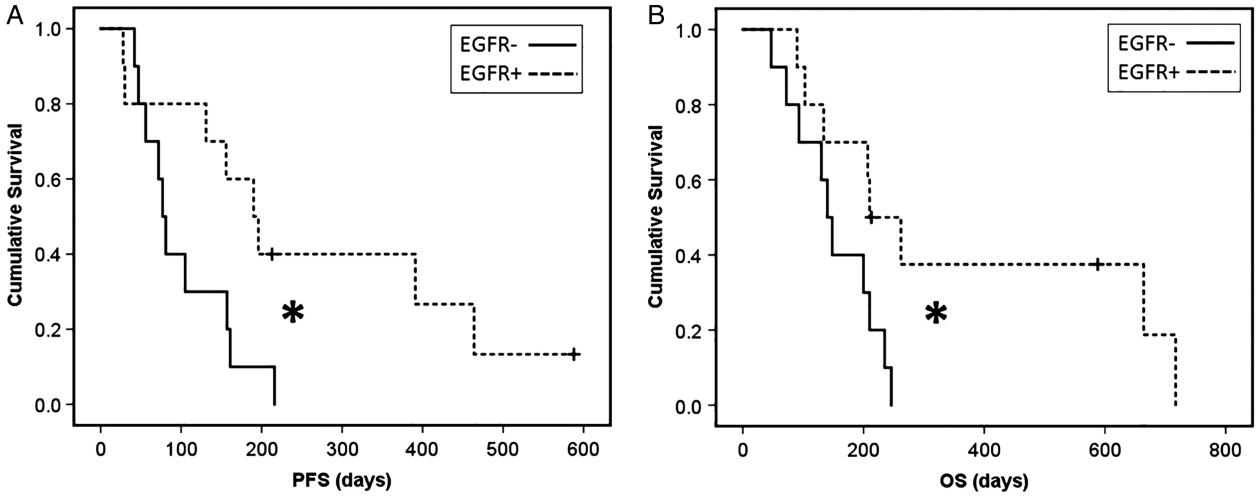

Fig. 4. Stratification of (A) PFS and (B) OS in EGFR+ and EGFR− patients following treatment with bevacizumab. *$P < .05$.

group with poorer PFS/OS and 4 were in the low RSI-FLAIR$_{90\%}$ change group with better PFS/OS). Despite proportional differences in group membership, a Wilcoxon rank-sum test did not reveal a significant difference in RSI-FLAIR$_{90\%}$ values between the EGFR+ and EGFR− patients [χ^2 (1) = .233, $P = .23$].

RSI versus High b-Value DWI

We repeated the CPH analysis with high b-value data (b = 4 000 only) and performed stepwise CPH models with both RSI and high b-value data in the model (see Supplementary Table). These results demonstrated that although high b-value DWI in the CE and FLAIR regions post-bevacizumab bears some association with survival that mirrors the RSI patterns, RSI values consistently show a *stronger* relationship to both PFS and OS ($P = .025–.044$ for high b-value DWI and 0.007–0.013 for RSI).

Discussion

Because anti-angiogenic therapy is widely used in patients with HGGs, and conventional imaging is limited in delineating true tumor response, identifying new, noninvasive imaging techniques that reliably predict response to anti-angiogenic therapy is of considerable importance. In this paper, we demonstrate that RSI, an advanced diffusion technique, can improve the prediction of both PFS and OS following bevacizumab relative to measures derived from standard diffusion imaging, CE, and FLAIR. In particular, we demonstrate that within the first 1–2 months following initiation of bevacizumab, an increase in RSI-derived measures of cellularity within the FLAIR/T2 region is the strongest predictor of poor PFS and OS. This association also holds within the CE region for OS. Although decreased ADC in the FLAIR/T2 region was associated with poorer OS, we contend that the weaker association between decreases in ADC and patient outcomes (based on both the stepwise CPH model and weaker *P*-values for ADC [$P = .035–.041$] compared with RSI [$P = .004–.007$]) is due to ADC's high sensitivity to bevacizumab-induced reduction in edema. This is further demonstrated by the fact that ADC decreased in the vast majority of patients post-bevacizumab in both the CE and FLAIR/T2 regions regardless of patient outcomes, and this decrease in ADC was correlated with the decrease in FLAIR/T2 volume (Fig. 2). Conversely, RSI values only increased in the FLAIR/T2 region, and this increase was not associated with FLAIR/T2 volume changes. Thus, by removing the fast, extracellular volume fraction associated with edema, RSI may provide a more stable and reliable estimate of changes in tumor cellularity, which could translate to a more accurate measure of treatment response.

It is noteworthy that our primary findings for both RSI and ADC were related to changes within the FLAIR/T2 region post-bevacizumab. These results parallel those of previous studies that found the 10th percentile of the ADC histogram post-bevacizumab[7] or the ratio of a lower ADC peak to a middle ADC peak using a 4-component curve-fit model[17] in the FLAIR/T2 region best stratified patients according to survival. Similarly, researchers have shown that the volume of the low ADC within the FLAIR/T2 region gradually increases following treatment with anti-angiogenic agents in a sizable subset of patients.[22,27] These findings add to existing evidence that while bevacizumab may control disease in the CE region, it leads to nonenhancing, infiltrative tumor growth that likely contributes to unfavorable patient outcomes. This hypothesis is strengthened by preclinical studies in mouse glioma models that suggest that blocking VEGF leads to a more infiltrative pattern of tumor growth.[37,38] Thus, due to the blockage of angiogenesis, tumor cells grow along existing brain blood vessels in a process called vascular cooption, which allows them to maintain an adequate blood supply. This has been validated in early human studies, which indicate that increases in FLAIR/T2 likely represent tumor invasion and vascular cooption.[29,39] Although there is some controversy as to whether this infiltrative pattern of tumor growth represents a more aggressive[7,28] or a less aggressive[27] phenotype, these data converge on the notion that measuring diffusion changes within the nonenhancing region is important in predicting prognosis following treatment with anti-angiogenic agents. Our data provide evidence that RSI may improve quantification of tumor burden in this region and could provide an early biomarker of bevacizumab-related tumor infiltration.

Recent data derived from traditional and graded fDMs have argued that changes within both the CE and FLAIR/T2 regions are critical to evaluating bevacizumab-related treatment response. Ellingson et al[18] reported that the volume of decreasing ADC within both the CE and FLAIR/T2 regions stratified patients with GBM according to OS. However, decreasing ADC within the CE region was a stronger predictor, which the authors attribute to the higher percentage of solid tumor in CE compared with FLAIR/T2 regions. In a second study,[21] however, they found that the rate of change in *hypercellular volume* (ie, low ADC) within the FLAIR/T2 region was a strong predictor of response to therapy in a mixed group of patients with HGG. Based on these results, they contend that measuring change in ADC within the CE region may be sufficient for GBM, but limited in patients with grade III tumors who may lack sizable CE. Although we observed that increases in RSI in both the CE and FLAIR/T2 regions were associated with poorer OS, RSI increases in the FLAIR/T2 region within the first 1–2 months following initiation of bevacizumab were a more reliable indicator of progression, whereas changes were less frequently observed in CE regions.

RSI versus High b-Value DWI

In addition to an advantage over ADC, our data revealed that RSI bears a stronger relationship with survival compared with high b-value DWI. These findings complement our previous work,[25] suggesting that RSI offers a unique advantage over standard and high b-value DWI by not only attenuating the signal associated with edema, but also attenuating restricted anisotropic water in normal-appearing white matter, which may allow for a more specific measure of restricted isotropic water associated with the presence of tumor cells.

EGFR Status and PFS/OS

It is well established that GBM tumors are genetically diverse and that patients with these tumors can be subdivided based on their molecular signature,[40] which may subsequently influence prognosis.[41] Thus, there is great interest in whether these molecular markers have a typical MRI phenotype that can add to the prediction of treatment response. EGFR amplification is commonly seen in GBM and known to affect downstream cellular processes, including angiogenesis.[42] However, the effects of EGFR amplification on survival and response to therapy are still debated.[43] In a post-hoc analysis, we found that EGFR+ status was associated with prolonged PFS and OS compared with EGFR− status following treatment with bevacizumab. However, EGFR status did not add to the prediction of survival above and beyond the change in RSI values. Because EGFR amplification may affect angiogenesis,[43] it is plausible that EGFR status could influence response to anti-angiogenic agents.

Limitations and Conclusions

Our sample size was relatively small and from a single institution. This reflected our attempt to perform a highly controlled study in which all patients were scanned on the same MR scanner with exactly the same imaging protocol. However, the generalizability of our results will need to be tested in prospective, multisite clinical trials across multiple vendor platforms. Second, we chose to analyze changes in our imaging metrics using a VOI rather than voxelwise approach. It is possible that voxelwise changes in RSI may provide an even more robust predictor of survival than change in RSI percentiles from histogram analysis. However, longitudinal registration of diffusion data is challenging in the context of major changes in edema, even when nonlinear algorithms are employed. Therefore, we selected a VOI approach that has shown robust results in previous studies[7,20] and does not depend on voxelwise tissue matching between timepoints. Because data were not collected as part of a prospective, clinical trial, there was significant treatment variability across patients in terms of both initial and follow-up treatments. In particular, multiple chemotherapeutic regimens were used in combination with bevacizumab in most patients and these different regimens could have differentially impacted patient outcomes. However, our most important finding is based on the prognostic advantage of RSI versus ADC *within* patients, which is not confounded by between-subject treatment variance. We also included a mixed group of patients with HGGs in our study. Although this approach was selected in efforts to increase the generalizability of our imaging technique to all HGGs, it also limits what can be concluded about the use of RSI in a more homogeneous patient group. Other potential limitations include the long scan time needed to acquire the RSI sequence (ie, 8 min for this study) and the additional postprocessing of the data. It should be noted that the RSI sequence takes only 4–5 min on many newer MRI systems. Additionally, the postprocessing of the data at our institution is now completely automated at the time of the scan, and the postprocessed RSI-CMs (shown in Fig. 1) are pushed back to PACS (picture archiving and communication system) for real-time review by the neuroradiologist.

In summary, our study emphasizes the value of an advanced diffusion technique, RSI, for quantifying response to therapy in patients treated with bevacizumab, especially in nonenhancing regions likely reflecting infiltrative tumor. We contend that by removing the hindered diffusion associated with edema, RSI provides a more direct measure of cellularity relative to ADC, which may translate to a more powerful biomarker of true tumor response to anti-angiogenic agents. This unique property of RSI may position it as a robust quantitative imaging tool for evaluating tumor response across a range of HGG treatments, both at the individual patient level and in large-scale clinical trials.

Supplementary Material

Supplementary material is available online at *Neuro-Oncology* (http://neuro-oncology.oxfordjournals.org/).

Funding

This work was supported by National Institutes of Health grants R01NS065838 (C.R.M.), RC2 DA29475 (A.M.D.), and EB00790-06 (A.M.D.); National Cancer Institute Cancer Center Specialized Grant (P30CA023100; C.R.M.); National Science Foundation Grant 1430082

(N.S.W.); National Institutes of Health UL1TR000100 (J.A.H.) and KL2TR00099 (J.A.H.); American Cancer Society Award ACS-IRG 70-002 (J.A.H.); and American Cancer Society Research Scholar Grant RSG-15-229-01-CCE (C.R.M.).

Acknowledgments

We would like to thank patients at the UCSD Moores Cancer Center Neuro-Oncology Program for their generous participation.

Conflict of interest statement. None of the authors have any personal or financial interest in drugs, materials, or devices described in this submission. There is a pending US application filled on RSI which is sponsored by UC San Diego (US13466081).

References

1. Greenlee RT, Murray T, Bolden S, et al. Cancer statistics, 2000. *CA Cancer J Clin*. 2000;50(1):7–33.
2. Stupp R, Mason WP, van den Bent MJ, et al. Radiotherapy plus concomitant and adjuvant temozolomide for glioblastoma. *N Engl J Med*. 2005;352(10):987–996.
3. Vredenburgh JJ, Desjardins A, Herndon JE 2nd, et al. Phase II trial of bevacizumab and irinotecan in recurrent malignant glioma. *Clin Cancer Res*. 2007;13(4):1253–1259.
4. Friedman HS, Prados MD, Wen PY, et al. Bevacizumab alone and in combination with irinotecan in recurrent glioblastoma. *J Clin Oncol*. 2009;27(28):4733–4740.
5. Kreisl TN, Kim L, Moore K, et al. Phase II trial of single-agent bevacizumab followed by bevacizumab plus irinotecan at tumor progression in recurrent glioblastoma. *J Clin Oncol*. 2009;27(5):740–745.
6. Clarke JL, Chang S. Pseudoprogression and pseudoresponse: challenges in brain tumor imaging. *Curr Neurol Neurosci Rep*. 2009;9(3):241–246.
7. Wen Q, Jalilian L, Lupo JM, et al. Comparison of ADC metrics and their association with outcome for patients with newly diagnosed glioblastoma being treated with radiation therapy, temozolomide, erlotinib and bevacizumab. *J Neurooncol*. 2015;121(2):331–339.
8. Wick W, Brandes AA, Gorlia T, et al. Phase III trial exploring the combination of bevacizumab and lomustine in patients with first recurrence of glioblastoma: The EORTC 26101 trial. *Neuro Oncol*. 2015;17(v1), doi: 10.1093/neuonc/nov306.
9. Gerstner ER, Frosch MP, Batchelor TT. Diffusion magnetic resonance imaging detects pathologically confirmed, nonenhancing tumor progression in a patient with recurrent glioblastoma receiving bevacizumab. *J Clin Oncol*. 2010;28(6):e91–e93.
10. Pope WB, Kim HJ, Huo J, et al. Recurrent glioblastoma multiforme: ADC histogram analysis predicts response to bevacizumab treatment. *Radiology*. 2009;252(1):182–189.
11. Chenevert TL, Stegman LD, Taylor JMG, et al. Diffusion magnetic resonance imaging: an early surrogate marker of therapeutic efficacy in brain tumors. *J Natl Cancer Inst*. 2000;92(24):2029–2036.
12. Jain R, Scarpace LM, Ellika S, et al. Imaging response criteria for recurrent gliomas treated with bevacizumab: role of diffusion weighted imaging as an imaging biomarker. *J Neurooncol*. 2010;96(3):423–431.
13. Sugahara T, Korogi Y, Kochi M, et al. Usefulness of diffusion-weighted MRI with echo-planar technique in the evaluation of cellularity in gliomas. *J Magn Reson Imaging*. 1999;9(1):53–60.
14. Chenevert TL, Sundgren PC, Ross BD. Diffusion imaging: insight to cell status and cytoarchitecture. *Neuroimaging Clin N Am*. 2006;16(4):619–632. viii–ix.
15. Pope WB, Lai A, Mehta R, et al. Apparent diffusion coefficient histogram analysis stratifies progression-free survival in newly diagnosed bevacizumab-treated glioblastoma. *AJNR Am J Neuroradiol*. 2011;32(5):882–889.
16. Ellingson BM, Sahebjam S, Kim HJ, et al. Pretreatment ADC histogram analysis is a predictive imaging biomarker for bevacizumab treatment but not chemotherapy in recurrent glioblastoma. *AJNR Am J Neuroradiol*. 2014;35(4):673–679.
17. Rahman R, Hamdan A, Zweifler R, et al. Histogram analysis of apparent diffusion coefficient within enhancing and nonenhancing tumor volumes in recurrent glioblastoma patients treated with bevacizumab. *J Neurooncol*. 2014;119(1):149–158.
18. Ellingson BM, Cloughesy TF, Lai A, et al. Graded functional diffusion map-defined characteristics of apparent diffusion coefficients predict overall survival in recurrent glioblastoma treated with bevacizumab. *Neuro Oncol*. 2011;13(10):1151–1161.
19. Ellingson BM, Cloughesy TF, Lai A, et al. Nonlinear registration of diffusion-weighted images improves clinical sensitivity of functional diffusion maps in recurrent glioblastoma treated with bevacizumab. *Magn Reson Med*. 2012;67(1):237–245.
20. Ellingson BM, Kim E, Woodworth DC, et al. Diffusion MRI quality control and functional diffusion map results in ACRIN 6677/RTOG 0625: a multicenter, randomized, phase II trial of bevacizumab and chemotherapy in recurrent glioblastoma. *Int J Oncol*. 2015;46(5):1883–1892.
21. Ellingson BM, Malkin MG, Rand SD, et al. Volumetric analysis of functional diffusion maps is a predictive imaging biomarker for cytotoxic and anti-angiogenic treatments in malignant gliomas. *J Neurooncol*. 2011;102(1):95–103.
22. Zhang M, Gulotta B, Thomas A, et al. Large-volume low lesion predicts poor survival in bevacizumab-treated glioblastoma patients. *Neuro Oncol*. 2015;18(5):735–743.
23. Pope WB, Qiao XJ, Kim HJ, et al. Apparent diffusion coefficient histogram analysis stratifies progression-free and overall survival in patients with recurrent GBM treated with bevacizumab: a multi-center study. *J Neurooncol*. 2012;108(3):491–498.
24. White NS, Leergaard TB, D'Arceuil H, et al. Probing tissue microstructure with restriction spectrum imaging: histological and theoretical validation. *Hum Brain Mapp*. 2013;34(2):327–346.
25. White NS, McDonald CR, Farid N, et al. Improved conspicuity and delineation of primary and metastatic brain tumors using "restriction spectrum imaging": quantitative comparison with high b-value DWI and ADC. *Am J Neuroradiol*. 2013;34(5):958–964.
26. Kothari PD, White NS, Farid N, et al. Longitudinal restriction spectrum imaging is resistant to pseudoresponse in patients with high-grade gliomas treated with bevacizumab. *AJNR Am J Neuroradiol*. 2013;34(9):1752–1757.
27. Gerstner ER, Chen PJ, Wen PY, et al. Infiltrative patterns of glioblastoma spread detected via diffusion MRI after treatment with cediranib. *Neuro Oncol*. 2010;12(5):466–472.
28. Norden AD, Young GS, Setayesh K, et al. Bevacizumab for recurrent malignant gliomas: efficacy, toxicity, and patterns of recurrence. *Neurology*. 2008;70(10):779–787.

29. Sorensen AG, Batchelor TT, Wen PY, et al. Response criteria for glioma. *Nat Clin Pract Oncol*. 2008;5(11):634–644.
30. Farid N, Almeida-Freitas DB, White NS, et al. Combining diffusion and perfusion differentiates tumor from bevacizumab-related imaging abnormality (bria). *J Neurooncol*. 2014;120(3):539–546.
31. McDonald CR, White NS, Farid N, et al. Recovery of white matter tracts in regions of peritumoral FLAIR hyperintensity with use of restriction spectrum imaging. *AJNR Am J Neuroradiol*. 2013;34(6):1157–1163.
32. Wen PY, Macdonald DR, Reardon DA, et al. Updated response assessment criteria for high-grade gliomas: response assessment in neuro-oncology working group. *J Clin Oncol*. 2010;28(11): 1963–1972.
33. Holland D, Kuperman JM, Dale AM. Efficient correction of inhomogeneous static magnetic field-induced distortion in Echo Planar Imaging. *Neuroimage*. 2010;50(1):175–183.
34. Padhani AR, Liu G, Koh DM, et al. Diffusion-weighted magnetic resonance imaging as a cancer biomarker: consensus and recommendations. *Neoplasia*. 2009;11(2):102–125.
35. White NS, McDonald C, Farid N, et al. Diffusion-weighted imaging in cancer: physical foundations and applications of restriction spectrum imaging. *Cancer Res*. 2014;74(17):4638–4652.
36. Yamasaki F, Kurisu K, Aoki T, et al. Advantages of high b-value diffusion-weighted imaging to diagnose pseudo-responses in patients with recurrent glioma after bevacizumab treatment. *Eur J Radiol*. 2012;81(10):2805–2810.
37. Jain RK, di Tomaso E, Duda DG, et al. Angiogenesis in brain tumours. *Nat Rev Neurosci*. 2007;8(8):610–622.
38. Kunkel P, Ulbricht U, Bohlen P, et al. Inhibition of glioma angiogenesis and growth in vivo by systemic treatment with a monoclonal antibody against vascular endothelial growth factor receptor-2. *Cancer Res*. 2001;61(18):6624–6628.
39. de Groot JF, Fuller G, Kumar AJ, et al. Tumor invasion after treatment of glioblastoma with bevacizumab: radiographic and pathologic correlation in humans and mice. *Neuro Oncol*. 2010; 12(3):233–242.
40. Ellingson BM. Radiogenomics and imaging phenotypes in glioblastoma: novel observations and correlation with molecular characteristics. *Curr Neurol Neurosci Rep*. 2015;15(1):506.
41. Ellison DW. Multiple molecular data sets and the classification of adult diffuse gliomas. *N Engl J Med*. 2015;372(26):2555–2557.
42. Carpenter G, Cohen S. Epidermal growth factor. *J Biol Chem*. 1990; 265(14):7709–7712.
43. Aghi M, Gaviani P, Henson JW, et al. Magnetic resonance imaging characteristics predict epidermal growth factor receptor amplification status in glioblastoma. *Clin Cancer Res*. 2005; 11(24 Pt 1):8600–8605.